



Published in final edited form as:

*Science*. 2017 April 21; 356(6335): 328–332. doi:10.1126/science.aai8764.

## Microtubules acquire resistance from mechanical breakage through intraluminal acetylation<sup>#</sup>

Zhenjie Xu<sup>1,2,\*</sup>, Laura Schaedel<sup>3</sup>, Didier Portran<sup>1</sup>, Andrea Aguilar<sup>1</sup>, Jérémie Gaillard<sup>3</sup>, M. Peter Marinkovich<sup>2,4</sup>, Manuel Théry<sup>3,5</sup>, and Maxence V. Nachury<sup>1,\*</sup>

<sup>1</sup>Department of Molecular and Cellular Physiology, Stanford University School of Medicine, Stanford, CA 94305-5345, USA

<sup>2</sup>Program in Epithelial Biology, Stanford University School of Medicine, Stanford, CA 94305-5168, USA

<sup>3</sup>CytoMorpho Lab, LPCV, UMR5168, Biosciences & Biotechnology Institute of Grenoble, CEA/INRA/CNRS/Université Grenoble-Alpes, 17 rue des Martyrs, 38054 Grenoble, France

<sup>4</sup>Division of Dermatology, Palo Alto VA Medical Center, Palo Alto, CA 94305, USA

<sup>5</sup>CytoMorpho Lab, A2T, UMRS1160, Institut Universitaire d'Hématologie, Hôpital Saint Louis, INSERM/AP-HP/Université Paris Diderot, 1 Avenue Claude Vellefaux, 75010 Paris, France

### Abstract

Eukaryotic cells rely on long-lived microtubules for intracellular transport and as compression-bearing elements. Intriguingly, long-lived microtubules are acetylated inside their lumen and microtubule acetylation has been proposed to modify microtubule mechanics. Here we found that tubulin acetylation is required for the mechanical stabilization of long-lived microtubules in cells. Depletion of the tubulin acetyltransferase TAT1 led to a significant increase in the frequency of microtubule breakage and nocodazole-resistant microtubules lost upon removal of acetylation were largely restored by either pharmacological or physical removal of compressive forces. In vitro reconstitution experiments demonstrated that acetylation is sufficient to protect microtubules from mechanical breakage. Thus, acetylation increases mechanical resilience to ensure the persistence of long-lived microtubules.

---

<sup>#</sup>This manuscript has been accepted for publication in *Science*. This version has not undergone final editing. Please refer to the complete version of record at <http://www.sciencemag.org/>. The manuscript may not be reproduced or used in any manner that does not fall within the fair use provisions of the Copyright Act without the prior, written permission of AAAS.

\*Correspondence: To whom correspondence should be addressed. [nachury@gmail.com](mailto:nachury@gmail.com), [zhenjie.xu@gmail.com](mailto:zhenjie.xu@gmail.com).

#### SUPPLEMENTARY MATERIALS

Materials and Methods

Supplementary Text

Figs. S1 to S12

References (33–50)

Movies S1 to S13.

## Main Text

How some cytoplasmic microtubules are stabilized and persist for several hours remains an open question (1). After stabilization, microtubules are post-translationally detyrosinated and acetylated on lysine 40 of  $\alpha$ -tubulin ( $\alpha$ K40). While detyrosination alters the binding site for microtubule associated proteins (MAPs), severing enzymes and motors to create specialized microtubule tracks (2), the molecular consequences of  $\alpha$ K40 acetylation remain elusive and it is difficult to conceptualize how the modification of a residue inaccessible from outside the microtubule could alter MAP and motor binding (2, 3). We recently proposed that acetylation modifies microtubule mechanics by weakening interprotofilament interactions (4)

TAT1 is responsible for nearly all acetylation on  $\alpha$ K40 in every organism studied (2). Although TAT1 depletion from RPE cells did not measurably affect global microtubule polymerization or organization (Fig. S1), tubulin detyrosination was significantly decreased at the bulk level (Fig. 1A and S2A–B) and reduced on microtubules of TAT1-depleted cells (Fig. 1B) and *Tat1*<sup>-/-</sup> MEFs (Fig. S2C). Given that acetylation and detyrosination sites are separated by the microtubule wall, it is unlikely that the two modifications are enzymatically coupled. Instead, long-lived microtubules, including detyrosinated microtubules, may be lost when acetylation is reduced. After treating cells with nocodazole, dynamic microtubules were depolymerized and most remaining microtubules displayed the typical characteristics of long-lived microtubules with high levels of acetylation and detyrosination and long and curly morphology (Fig. 1C and S2D). Under the same conditions, very few microtubules remained in TAT1-depleted cells and these were very short, dispersed throughout the cell and devoid of detyrosinated tubulin (Fig. 1C). The number of microtubules that remained after nocodazole treatment was significantly decreased upon TAT1 depletion in RPE cells (Fig. 1D) or in *Tat1*<sup>-/-</sup> MEFs (Fig. S2E–F). The effect of TAT1 removal was even more striking when the length of nocodazole-resistant microtubules was examined (Fig. 1E). After 60 min of nocodazole treatment, most microtubules were normally longer than 4  $\mu$ m, but shorter than 2  $\mu$ m in TAT1-depleted cells.

Because pharmacological reduction of tubulin detyrosination did not affect the length of nocodazole-resistant microtubules or the levels of acetylation (Fig. S3), the effect of TAT1 depletion on nocodazole-resistant microtubules are unlikely to be caused by the observed reduction in detyrosination. Because overexpression of TAT1 –but not a catalytically dead mutant– significantly elevated the mass of nocodazole-resistant microtubules (Fig. S4) and because nocodazole-resistant microtubules are increased in MEFs that lack the tubulin deacetylase HDAC6 (5), it is  $\alpha$ K40 acetylation rather than an acetyltransferase-independent activity of TAT1 (6–8) that is required for the maintenance of long-lived cytoplasmic microtubules in mammalian cells. Long-lived microtubules are not lost from TAT1-depleted cells due to an increased susceptibility to severing enzymes because acetylation does not influence the activity of spastin *in vitro* (9) and did not affect the activity of spastin or katanin *in vivo* (Fig. S5). Defective centrosomal microtubule anchoring in TAT1-depleted cells was ruled out by imaging microtubule re-growth after depolymerization (Fig. S6).

Long-lived microtubules display frequent buckling because of compressive forces generated by microtubule-based motors and actomyosin contractility (10–12). Because microtubules are very stiff polymers that rupture when subjected to flexural stresses (13), this highly bent morphology suggests the existence of protective mechanisms for long-lived microtubules. The repair of lattice defects has emerged as an intrinsic property of microtubules that are subjected to mechanical stress (14, 15) and acetylation protects microtubule from mechanical fatigue in vitro (4). Further suggesting that acetylation may confer mechanical protection to microtubules, removing TAT-1 from touch receptor neurons of nematodes results in profound microtubule lattice defects (6, 16) that can be rescued by paralyzing the animals (8). Finally, while detyrosination is evenly distributed along microtubules (Fig. S7A) (17), the pattern of acetylation is discontinuous with a preference for highly curved areas of nocodazole-resistant microtubules (Fig. 1F–G and S7B), suggesting that TAT1 may preferentially acetylate segments experiencing stress. Alternatively, it is conceivable that only bends at regions that are acetylated were preserved after fixation (see Supplementary Text). Localized acetylation is thus a prime candidate for the mechanical adaptation of microtubules to mechanical stresses.

We sought to test the hypothesis that long-lived microtubules disappear in the absence of TAT1 because of an increase rate of breakage under mechanical stress. In the past, imaging of microtubules breakage has been limited to very thin areas of the cell such as lamellipodia where single microtubules can be readily resolved (11, 18, 19). However, most of the microtubules in lamellipodia are dynamic and thus not acetylated (20). To specifically image the breakage of long-lived microtubules, we followed microtubules in real time in the presence of nocodazole using a triple GFP fusion with the microtubule-binding domain of esconsin (EMTB), a MAP that does not affect microtubule dynamics when expressed at low levels (21). After 15 min in nocodazole, most remaining microtubules were highly bent, acetylated and detyrosinated (Fig. S7A) and microtubule number was similar in control- and TAT1-depleted RPE-[EMTB-GFP<sup>3</sup>] cells (Fig. S8A–B). Over the next 30 min of live cell imaging, microtubules rapidly disappeared in TAT1-depleted cells whereas most microtubules persisted in control-depleted cells (Fig. S8A and C) and the mean microtubule length was significantly decreased in TAT1-depleted cells after 50 min in nocodazole (Fig. S8D). Consistent with prior observations of microtubule breakage in fibroblasts (18, 19), typical rupture events (Fig. 2A–C, S9A–B and Movies S5–S9) were preceded by local microtubule buckling with the breakage site coinciding with the region of highest curvature. Tracking individual microtubules demonstrated that the frequency of microtubule breakage events preceded by buckling was increased 2-fold in TAT1-depleted cells compared to control-depleted cells (Fig. 2D). The frequency of microtubule breakage events that were not preceded by buckling (shown in Fig. S9C and Movie S10) showed no significant difference between control- and TAT1-depleted cells (Fig. S9D). These findings suggest that tubulin acetylation protects microtubules from breakage resulting from compressive forces.

The two known types of forces responsible for buckling and breakage of cytoplasmic microtubules are microtubule motors pushing onto anchored microtubules (11) and actomyosin contractility transmitted through actin-microtubule linker proteins (19). Contractility is likely to represent the major factor responsible for microtubule compression in nocodazole-treated cells because microtubule depolymerization leads to activation of Rho

and Rho Kinase (ROCK) thereby increasing myosin activity and stress fiber assembly (22). To test the hypothesis that long-lived microtubules in TAT1-depleted cells break under actomyosin-mediated compression, we treated cells with the ROCK inhibitor Y27632 or the myosin inhibitor blebbistatin and then removed dynamic microtubules using nocodazole (Fig. 3A, S10 and S11). Pharmacological release of tension increased the mean length of nocodazole-resistant microtubules 1.5-fold in control-depleted cells (Fig. 3B). The effect of Y27632 on TAT1-depleted cells was much more dramatic with the mean length of nocodazole-resistant microtubules increasing 4-fold (Fig. 3B) and the length distribution of nocodazole-resistant microtubules approaching that of control-depleted cells in the absence of Y27632 (Fig. 3B). A statistical test for the rescue of microtubule length in TAT1-depleted cells was highly significant with Y27632 (Fig. 3B) and significant with blebbistatin (Fig. S11). ROCK inhibition did not restore tubulin acetylation in TAT1-depleted cells (Fig. S10B and C). Thus, inhibition of the major Rho effectors largely restores the nocodazole-resistant microtubules lost from TAT1-depleted cells.

Since ROCK inhibition may stabilize microtubules in TAT1-depleted cells through other mechanisms than the release of compressive forces (e.g. inhibitory phosphorylation of MAPs (23)), we sought to release the compressive forces exerted onto microtubules in a more direct and specific manner. When cells are plated onto soft substrates made of fibronectin-coated polyacrylamide (24, 25) (Fig. 3C and S12), the force-dependent maturation of focal adhesions is stunted, stress fiber assembly is limited and contractility is low (25). Plating cells on polyacrylamide largely rescued the length of nocodazole-resistant microtubules in TAT1-depleted cells (Fig. 3D). Meanwhile, the length of nocodazole-resistant microtubules was not significantly changed by plating control cells on polyacrylamide gel thus indicating that adhesion signaling does not affect long-lived microtubules under these experimental conditions (Fig. 3D and S12D). Together, the partial rescue of microtubule length by pharmacological and physical treatments strongly suggests that acetylation protects long-lived microtubules from breakage resulting from the compressive forces generated by the actomyosin cytoskeleton and makes it unlikely that acetylation prevents nocodazole-induced depolymerization. The observation that microtubule length is not fully rescued is consistent with residual forces (e.g. microtubule motors) applying stress on microtubules after these treatments.

Considering that most tissues have the stiffness of polyacrylamide gels, the observation that nocodazole-resistant microtubules are largely immune to TAT1 depletion when cells are plated on polyacrylamide gels provides a cogent explanation for the very mild phenotypes of *Tat1*<sup>-/-</sup> mice. The marked effects of TAT1 depletion when cells are plated on glass suggest that TAT1 will be required in specialized cell types where the stiffness is considerably higher than a few kPa (e.g. bone) or where microtubules are subjected to repeated mechanical stresses. Congruent with the latter hypothesis, microtubules appear damaged in touch receptor neurons of nematodes that lack TAT-1 (16, 26) and tubulin acetylation sets the optimal cell stiffness for touch sensation in mammalian mechanosensory neurons (27). Further work examining microtubule breakage in these specialized settings is needed to establish the role of tubulin acetylation in physiological contexts.

Because some MAPs can change the mechanical properties of microtubules (28, 29), acetylation could confer mechanical resistance to microtubules by altering the recruitment of specific MAPs. Alternatively, acetylation may change interactions within the lattice to directly alter microtubule mechanics (4). To determine if acetylation directly protects microtubules from physical rupture, we generated pure preparations of enzymatically acetylated and de-acetylated microtubules (4) and reconstituted microtubule breakage *in vitro* using a modification of our microfluidics- and micropatterning-based microtubule bending system (14) (Fig. 4A). First, we confirmed that flexural rigidity is decreased by acetylation (Fig. 4B–C) (4). By including large stationary beads in the path of the bending microtubules, the microtubule sharply kinked and frequently broke at the site of maximal curvature (Fig. 4D). While nearly a third of the deacetylated microtubules ( $Ac^1$ ) ruptured under the mechanical stress, only 2% of the highly acetylated microtubules ( $Ac^{97}$ ) broke under the same conditions (Fig. 4E). Thus, acetylation directly protects microtubules from rupture. We propose that, by weakening interprotofilament interactions (4), acetylation increases lattice plasticity and limits the spread of preexisting lattice damage under repeated mechanical stress, thus protecting microtubules from material fatigue (4) or mechanical breakage (Fig. 4E). Because acetylation is enriched in regions of high curvature (Fig. 1G), microtubule mechanics are likely to be modified locally. Furthermore, cyclic stretch of cells increases acetylation (30) and lattice openings are found in bent segments of microtubules (31). Stress-induced bending may thus produce transient openings that let TAT1 access the microtubule lumen in areas experiencing the highest stress (32) and result in an adaptive and local increase in mechanical resilience (Fig. 4F).

## Supplementary Material

Refer to Web version on PubMed Central for supplementary material.

## Acknowledgments

We are grateful to Z. Werb for hosting experiments in her lab, S. Triclin and L. Kurzawa for investigating microtubule lifetime in TAT1-depleted cells, D. Nager and F. Ye for assistance with statistical analysis, T. Vignaud and Q. Tseng for preparing polyacrylamide coated coverslips, to G.G. Gundersen for the deetyrosinated tubulin antibody, to C. Bulinski for p3xGFP-EMTB, to C. Janke for the spastin cDNA and to F. McNally for the katanin p60 construct. This work was funded by Stanford SoM (Deans' Fellowships to Z.X. and A.A.), NIH-NCI (CA108462, Z.X.), DoD (BC103963, Z.X.), HFSP (RGY0088, M.V.N. and M.T), ANR (14-CE09-0014-02, M.T.) and the Palo Alto VA (M.P.M.). M.V.N., M.T. and Z.X. conceived and coordinated the project with help from M.P.M; M.V.N. and Z.X. wrote the paper with contributions from all authors; L.S., M.T. and J.G. developed the microfluidics system and performed the bending and breakage experiments, D.P. prepared tubulin with defined acetylation level, A.A. conducted experiments with MEFs, and Z.X. conducted all other experiments. Data described can be found in the main figures and supplementary materials. The authors declare no conflict of interest.

## REFERENCES AND NOTES

1. Li R, Gundersen GG. Beyond polymer polarity: how the cytoskeleton builds a polarized cell. *Nat Rev Mol Cell Biol.* 2008; 9:860–873. [PubMed: 18946475]
2. Song Y, Brady ST. Post-translational modifications of tubulin: pathways to functional diversity of microtubules. *Trends Cell Biol.* 2015; 25:125–136. [PubMed: 25468068]
3. Janke C, Bulinski JC. Post-translational regulation of the microtubule cytoskeleton: mechanisms and functions. *Nat Rev Mol Cell Biol.* 2011; 12:773–786. [PubMed: 22086369]
4. Portran D, Schaedel L, Xu Z, They M, Nachury MV. Tubulin acetylation protects long-lived microtubules against mechanical ageing. *Nat Cell Biol.* 2017; 12:773.

5. Tran ADA, et al. HDAC6 deacetylation of tubulin modulates dynamics of cellular adhesions. *J Cell Sci.* 2007; 120:1469–1479. [PubMed: 17389687]
6. Topalidou I, et al. Genetically separable functions of the MEC-17 tubulin acetyltransferase affect microtubule organization. *Curr Biol.* 2012; 22:1057–1065. [PubMed: 22658602]
7. Kalebic N, et al. The Tubulin Acetyltransferase  $\alpha$ TAT1 Destabilizes Microtubules Independently of its Acetylation Activity. *Mol Cell Biol.* 2012; 33:1114–1123. [PubMed: 23275437]
8. Neumann B, Hilliard MA. Loss of MEC-17 leads to microtubule instability and axonal degeneration. *Cell Rep.* 2014; 6:93–103. [PubMed: 24373971]
9. Valenstein ML, Roll-Mecak A. Graded Control of Microtubule Severing by Tubulin Glutamylation. *Cell.* 2016; 164:911–921. [PubMed: 26875866]
10. Brangwynne CP, et al. Microtubules can bear enhanced compressive loads in living cells because of lateral reinforcement. *J Cell Biol.* 2006; 173:733–741. [PubMed: 16754957]
11. Bicek AD, et al. Anterograde microtubule transport drives microtubule bending in LLC-PK1 epithelial cells. *Mol Biol Cell.* 2009; 20:2943–2953. [PubMed: 19403700]
12. Robison P, et al. Detyrosinated microtubules buckle and bear load in contracting cardiomyocytes. *Science.* 2016; 352:aaf0659–aaf0659. [PubMed: 27102488]
13. Hawkins T, Mirigian M, Selcuk Yasar M, Ross JL. Mechanics of microtubules. *J Biomech.* 2010; 43:23–30. [PubMed: 19815217]
14. Schaedel L, et al. Microtubules self-repair in response to mechanical stress. *Nat Mater.* 2015; 14:1156–1163. [PubMed: 26343914]
15. Aumeier C, et al. Self-repair promotes microtubule rescue. *Nat Cell Biol.* 2016; 18:1054–1064. [PubMed: 27617929]
16. Cueva JG, Hsin J, Huang KC, Goodman MB. Posttranslational acetylation of  $\alpha$ -tubulin constrains protofilament number in native microtubules. *Curr Biol.* 2012; 22:1066–1074. [PubMed: 22658592]
17. Geuens G, et al. Ultrastructural colocalization of tyrosinated and detyrosinated alpha-tubulin in interphase and mitotic cells. *J Cell Biol.* 1986; 103:1883–1893. [PubMed: 3782287]
18. Odde DJ, Ma L, Briggs AH, DeMarco A, Kirschner MW. Microtubule bending and breaking in living fibroblast cells. *J Cell Sci.* 1999; 112(Pt 19):3283–3288. [PubMed: 10504333]
19. Gupton SL, Salmon WC, Waterman-Storer CM. Converging populations of f-actin promote breakage of associated microtubules to spatially regulate microtubule turnover in migrating cells. *Curr Biol.* 2002; 12:1891–1899. [PubMed: 12445381]
20. Ezratty EJ, Partridge MA, Gunderson GG. Microtubule-induced focal adhesion disassembly is mediated by dynamin and focal adhesion kinase. *Nat Cell Biol.* 2005; 7:581–590. [PubMed: 15895076]
21. Faire K, et al. E-MAP-115 (ensconsin) associates dynamically with microtubules in vivo and is not a physiological modulator of microtubule dynamics. *J Cell Sci.* 1999; 112(Pt 23):4243–4255. [PubMed: 10564643]
22. Chang YC, Nalbant P, Birkenfeld J, Chang ZF, Bokoch GM. GEF-H1 couples nocodazole-induced microtubule disassembly to cell contractility via RhoA. *Mol Biol Cell.* 2008; 19:2147–2153. [PubMed: 18287519]
23. Amano M, Nakayama M, Kaibuchi K. Rho-kinase/ROCK: A key regulator of the cytoskeleton and cell polarity. *Cytoskeleton.* 2010; 67:545–554. [PubMed: 20803696]
24. Pelham RJ, Wang YL. Cell locomotion and focal adhesions are regulated by substrate flexibility. *Proc Natl Acad Sci USA.* 1997; 94:13661–13665. [PubMed: 9391082]
25. Solon J, Levental I, Sengupta K, Georges PC, Janmey PA. Fibroblast adaptation and stiffness matching to soft elastic substrates. *Biophys J.* 2007; 93:4453–4461. [PubMed: 18045965]
26. Topalidou I, Chalfie M. Shared gene expression in distinct neurons expressing common selector genes. *Proc Natl Acad Sci U S A.* 2011; 108:19258–19263. [PubMed: 22087002]
27. Morley SJ, et al. Acetylated tubulin is essential for touch sensation in mice. *Elife.* 2016; 5:618.
28. Felgner H, et al. Domains of neuronal microtubule-associated proteins and flexural rigidity of microtubules. *J Cell Biol.* 1997; 138:1067–1075. [PubMed: 9281584]



29. Portran D, et al. MAP65/Ase1 promote microtubule flexibility. *Mol Biol Cell*. 2013; 24:1964–1973. [PubMed: 23615441]
30. Hoey DA, Hoey DA, Downs ME, Downs ME, Jacobs CR. The mechanics of the primary cilium: an intricate structure with complex function. *J Biomech*. 2012; 45:17–26. [PubMed: 21899847]
31. Schaap IAT, Carrasco C, de Pablo PJ, MacKintosh FC, Schmidt CF. Elastic response, buckling, and instability of microtubules under radial indentation. *Biophys J*. 2006; 91:1521–1531. [PubMed: 16731557]
32. Coombes C, et al. Mechanism of microtubule lumen entry for the  $\alpha$ -tubulin acetyltransferase enzyme  $\alpha$ TAT1. *Proc Natl Acad Sci U S A*. 2016; 113:E7176–E7184. [PubMed: 27803321]
33. Shida T, Cueva JG, Xu Z, Goodman MB, Nachury MV. The major alpha-tubulin K40 acetyltransferase alphaTAT1 promotes rapid ciliogenesis and efficient mechanosensation. *Proc Natl Acad Sci U S A*. 2010; 107:21517–21522. [PubMed: 21068373]
34. Lacroix B, et al. Tubulin polyglutamylation stimulates spastin-mediated microtubule severing. *J Cell Biol*. 2010; 189:945–954. [PubMed: 20530212]
35. McNally KP, Bazirgan OA, McNally FJ. Two domains of p80 katanin regulate microtubule severing and spindle pole targeting by p60 katanin. *J Cell Sci*. 2000; 113(Pt 9):1623–1633. [PubMed: 10751153]
36. Guarguaglini G, et al. The forkhead-associated domain protein Cep170 interacts with Polo-like kinase 1 and serves as a marker for mature centrioles. *Mol Biol Cell*. 2005; 16:1095–1107. [PubMed: 15616186]
37. Aguilar A, et al. A-tubulin K40 acetylation is required for contact inhibition of proliferation and cell-substrate adhesion. *Mol Biol Cell*. 2014; 25:1854–1866. [PubMed: 24743598]
38. Engler A, et al. Substrate compliance versus ligand density in cell on gel responses. *Biophys J*. 2004; 86:617–628. [PubMed: 14695306]
39. Khawaja S, Gundersen GG, Bulinski JC. Enhanced stability of microtubules enriched in detyrosinated tubulin is not a direct function of detyrosination level. *J Cell Biol*. 1988; 106:141–149. [PubMed: 3276710]
40. Kerr JP, et al. Detyrosinated microtubules modulate mechanotransduction in heart and skeletal muscle. *Nature Communications*. 2015; 6:8526.
41. Loktev AV, et al. A BBSome subunit links ciliogenesis, microtubule stability, and acetylation. *Dev Cell*. 2008; 15:854–865. [PubMed: 19081074]
42. Minotti AM, Barlow SB, Cabral F. Resistance to antimetabolic drugs in Chinese hamster ovary cells correlates with changes in the level of polymerized tubulin. *J Biol Chem*. 1991; 266:3987–3994. [PubMed: 1671676]
43. Gundersen GG, Kalnoski MH, Bulinski JC. Distinct populations of microtubules: tyrosinated and nontyrosinated alpha tubulin are distributed differently in vivo. *Cell*. 1984; 38:779–789. [PubMed: 6386177]
44. Bechstedt S, Lu K, Brouhard GJ. Doublecortin recognizes the longitudinal curvature of the microtubule end and lattice. *Curr Biol*. 2014; 24:2366–2375. [PubMed: 25283777]
45. Waterman-Storer CM, Salmon ED. Actomyosin-based retrograde flow of microtubules in the lamella of migrating epithelial cells influences microtubule dynamic instability and turnover and is associated with microtubule breakage and treadmilling. *J Cell Biol*. 1997; 139:417–434. [PubMed: 9334345]
46. Hyman A, et al. Preparation of modified tubulins. *Meth Enzymol*. 1991; 196:478–485. [PubMed: 2034137]
47. Polte TR, Eichler GS, Wang N, Ingber DE. Extracellular matrix controls myosin light chain phosphorylation and cell contractility through modulation of cell shape and cytoskeletal prestress. *Am J Physiol, Cell Physiol*. 2004; 286:C518–28. [PubMed: 14761883]
48. Beningo KA, Hamao K, Dembo M, Wang YL, Hosoya H. Traction forces of fibroblasts are regulated by the Rho-dependent kinase but not by the myosin light chain kinase. *Arch Biochem Biophys*. 2006; 456:224–231. [PubMed: 17094935]
49. Mazo G, Soplop N, Wang WJ, Uryu K, Tsou MFB. Spatial Control of Primary Ciliogenesis by Subdistal Appendages Alters Sensation-Associated Properties of Cilia. *Dev Cell*. 2016; 39:424–437. [PubMed: 27818179]

50. Piperno G, LeDizet M, Chang XJ. Microtubules containing acetylated alpha-tubulin in mammalian cells in culture. *J Cell Biol.* 1987; 104:289–302. [PubMed: 2879846]

Author Manuscript

Author Manuscript

Author Manuscript

Author Manuscript



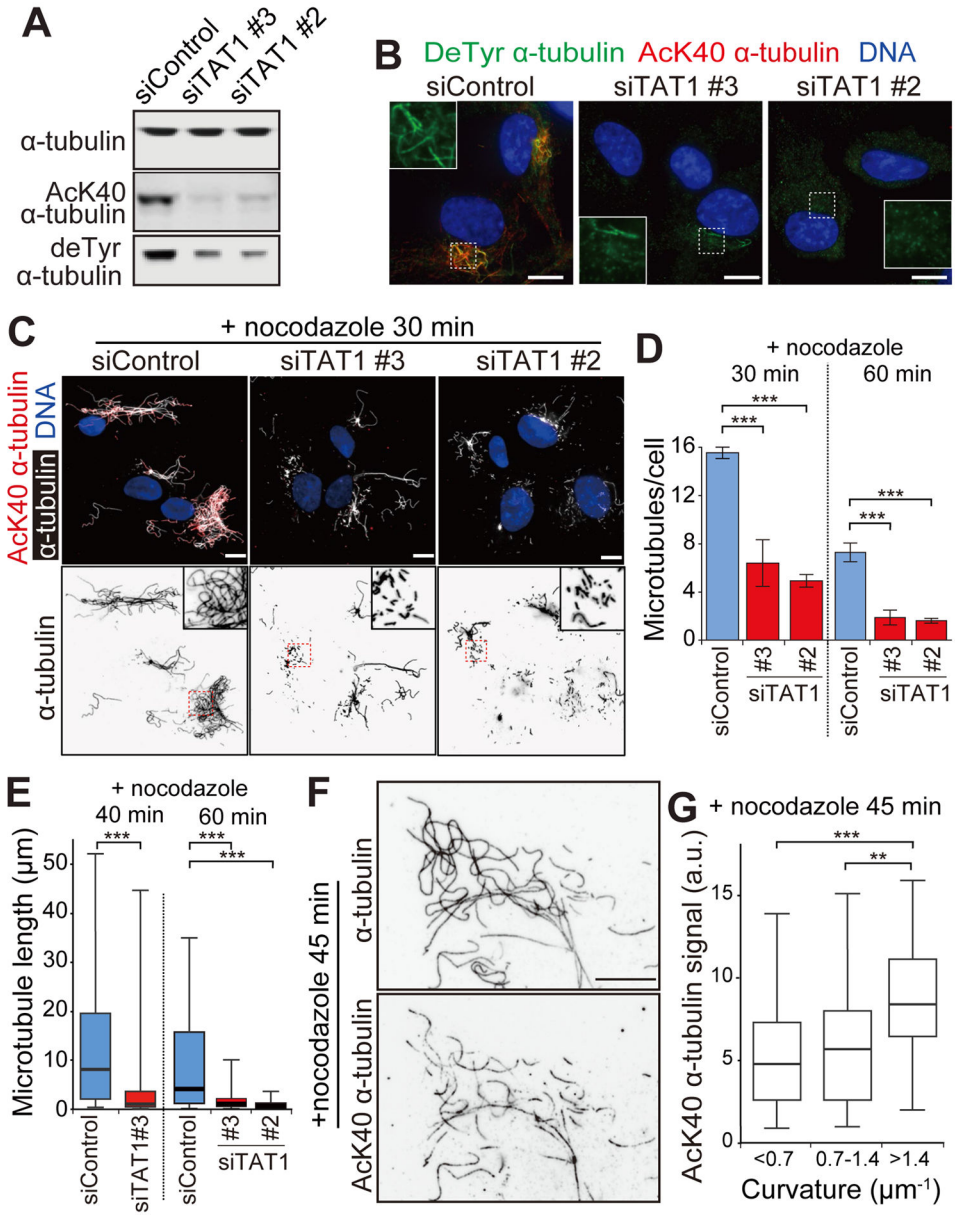


**Fig. 1. Long-lived microtubules are lost in the absence of  $\alpha$ -tubulin K40 acetylation**  
 (A)  $\alpha$ -tubulin K40 acetylation and detyrosination levels were measured by immunoblotting lysates of RPE cells treated with two different siRNAs against TAT1 (siTAT1#2 and siTAT1#3) or control siRNAs (siControl). (B) Immunofluorescence (IF) images of siRNA-treated RPE cells stained for acetylated  $\alpha$ -tubulin K40 (red), detyrosinated tubulin (green) and DNA (blue). Scale bar: 10  $\mu$ m. (C) IF images of siRNA-treated RPE cells treated with 2  $\mu$ M nocodazole and stained for  $\alpha$ -tubulin (white), acetylated  $\alpha$ -tubulin (red) and DNA (blue). Bottom panels show the  $\alpha$ -tubulin channel alone. Insets show the highly curved microtubules present in control-depleted cells and the very short microtubules in TAT1-depleted cells. Scale bar, 10  $\mu$ m (main panels). Insets are 10  $\times$  10  $\mu$ m. The number (D) and length (E) of microtubules remaining after nocodazole treatment were measured in siRNA-

treated RPE cells. **(D)**  $N(30 \text{ min}) = 153$  (siCTRL), 157 (siTAT1#3) and 155 (siTAT1#2) cells, 4 independent experiments;  $N(60 \text{ min}) = 236$  (siCTRL), 302 (siTAT1#3) and 206 (siTAT#2) cells, 3 independent experiments. Error bars indicate SD. Asterisks indicate  $t$  test significance values;  $***P < 10^{-4}$ . **(E)** The box is bound by the 25<sup>th</sup>–75<sup>th</sup> percentile, whiskers span 5<sup>th</sup> to 95<sup>th</sup> percentile and the bar in the middle is the median.  $N(40 \text{ min}) = 3,058$  (siControl), 4,659 (siTAT1#3) microtubules from at least 500 cells, 6 independent experiments;  $N(60 \text{ min}) = 880$  (siControl), 1,783 (siTAT1#3) and 1323 (siTAT1#2) microtubules from at least 180 cells, 3 independent experiments. Asterisks indicate Mann-Whitney  $U$  test significance values;  $***P < 10^{-4}$ . **(F)** IF images of RPE cells treated with nocodazole for 45 min and stained for acetylated  $\alpha$ -tubulin K40 and  $\alpha$ -tubulin. Scale bar, 10  $\mu\text{m}$ . **(G)** The level of  $\alpha$ -tubulin K40 acetylation and the curvature were measured along microtubules in IF images of cells treated with nocodazole for 45 min. The whiskers indicate 1.5 times the range.  $N = 1,904$  data points from 23 microtubules. Asterisks indicate Mann-Whitney  $U$  test significance values;  $**P < 10^{-3}$ ,  $***P < 10^{-4}$ .

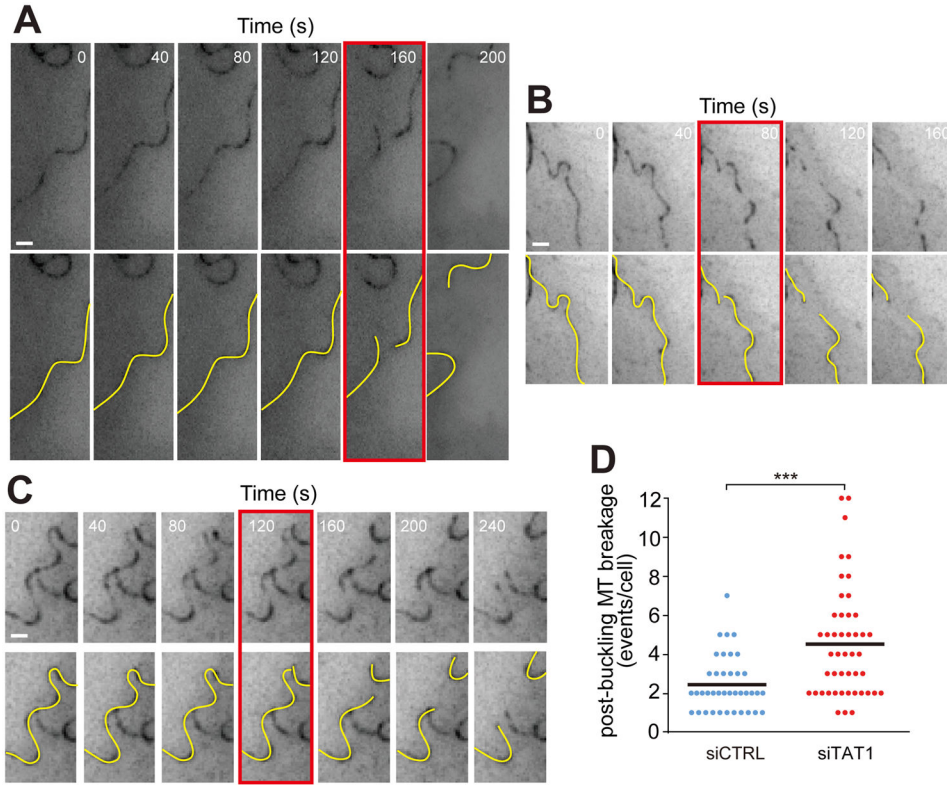


**Fig. 2. TAT1 depletion sensitizes nocodazole-resistant microtubules to mechanical breakage** (A–C) Microtubules were imaged in real-time in siRNA-treated RPE-[EMTB-GFP<sup>3</sup>] cells after at least 15 min in the presence of 2  $\mu$ M nocodazole. Projection images were generated to capture microtubules across the entire cell thickness and to avoid missing microtubule segments because they leave the focal plane. The yellow lines highlight microtubule behavior and the red box indicates the first frame where rupture is clearly detected. Scale bar, 1  $\mu$ m. The time series are extracted from Movies S5–S7. (D) Microtubule breakage events preceded by buckling were counted in control- and TAT1-depleted RPE-[EMTB-GFP<sup>3</sup>] cells during the 15 to 80 min period of nocodazole treatment.  $N = 46$  (siControl) and 52 (siTAT1) cells, 6 independent experiments. The bar marks the mean. Asterisks indicate  $t$  test significance values; \*\*\* $P < 10^{-4}$ .

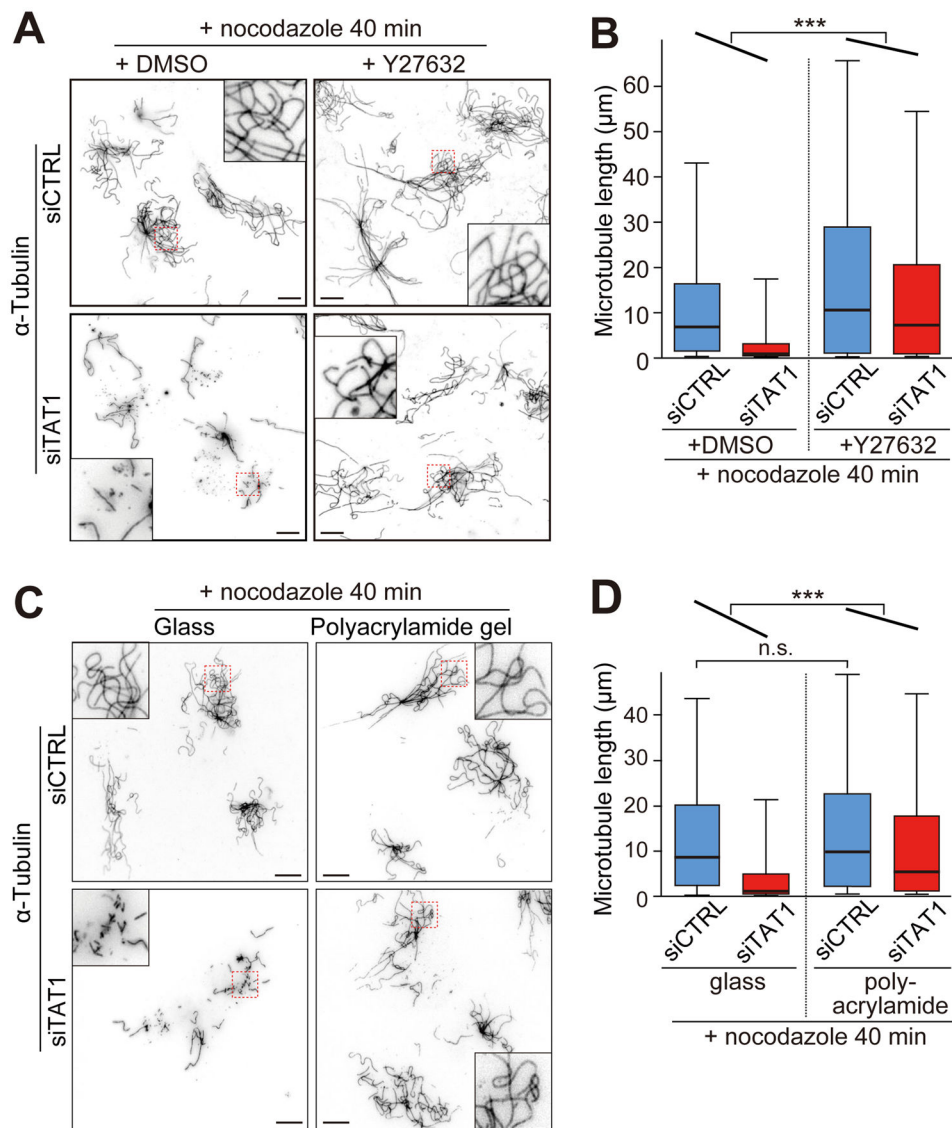


**Fig. 3. Release of cell tension restores the length of nocodazole-resistant microtubules in TAT1-depleted cells**

(A) Control- and TAT1-depleted cells were treated with Y27632 or vehicle for 1 h, then nocodazole was added for 40 min and cells were fixed and stained for α-tubulin. Insets show the detailed morphology of nocodazole-resistant microtubules. Scale bar: 10 µm. Insets are 10 × 10 µm. Cells before nocodazole treatment are shown in Fig. S10B. While Nocodazole-resistant microtubules are few and short in the absence of TAT1, the addition of Y27632 leads to the presence of numerous long nocodazole-resistant microtubules in TAT1-depleted cells. (B) Measurement of individual microtubule length. The box plots follow the same conventions as Fig. 1E.  $N = 128$  cells (2,371 microtubules) siControl/DMSO, 369 cells (2,879 microtubules) siTAT1/DMSO, 152 cells (2,462 microtubules) siControl/Y27632 and 359 cells (2,446 microtubules) siTAT1/Y27632, 3 independent experiments. Asterisks indicate multiple regression test significance values.  $***P < 10^{-4}$ . (C) Control- and TAT1-depleted cells plated on glass coverslips (elastic modulus 50 GPa) or polyacrylamide-gel (PA)

coated coverslips (elastic modulus 7 kPa) were treated with nocodazole for 40 min, fixed with PFA and stained for  $\alpha$ -tubulin. Insets show the detailed morphology of nocodazole-resistant microtubules. Scale bar: 10  $\mu\text{m}$  (main panels). Insets are 10  $\times$  10  $\mu\text{m}$ . Cells before nocodazole treatment are shown in Fig. S12. Nocodazole-resistant microtubules in TAT1-depleted cells are nearly absent when cells are plated onto glass but largely intact when cells are plated onto soft substrates. **(D)** Measurement of individual microtubule length. The box plots follow the same conventions as Fig. 1E.  $N = 1,489$  microtubules (siControl/glass), 2,201 (siTAT1/glass), 1,739 (siControl/PA) and 2,138 (siTAT1/PA), 3 independent experiments. Asterisks indicate multiple regression test significance values. \*\*\* $P < 10^{-4}$ . n.s. indicates Mann-Whitney  $U$  test significance value  $P > 0.01$ .



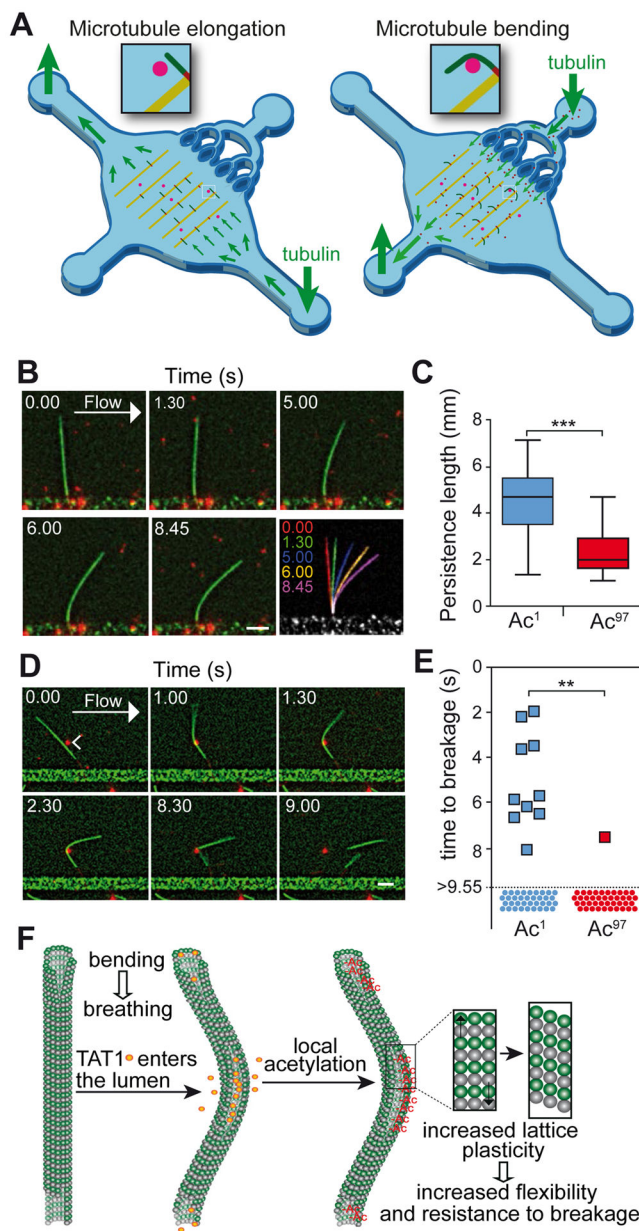


**Fig. 4. Acetylation protects microtubules from mechanical breakage**

(A) The microfluidic device used to reconstitute microtubule bending and breaking comprised two inlets and two outlets to control fluid flow along two orthogonal axes. By flowing them along the long axis, microtubule seeds (red) were grafted normally to the micropatterned lines, thus forcing microtubules to elongate parallel to the long axis. For the breakage assay, large beads (pink) that nonspecifically adhere to the surface were included to serve as fixed obstacles. A controlled fluid flow was applied along the short axis to subject microtubules to a normal bending force (right). The solution applied during the bending step contained free tubulin to keep microtubules dynamic and small beads (red) were added to the flowed solution to measure the flow in situ. (B) Time series showing the progressive bending of a microtubule (green) upon application of fluid flow. Scale bar: 5  $\mu\text{m}$ .

The pseudocolored image shows the overlay of successive time points. **(C)** Quantitation of the persistence length of microtubules made from enzymatically acetylated and deacetylated tubulin. The box plot follows the conventions of Fig. 1G. The levels of  $\alpha$ K40 acetylation were 97.2 % (Ac<sup>97</sup>) or 0.8 % (Ac<sup>1</sup>).  $N = 29$  (Ac<sup>1</sup>) and 25 (Ac<sup>97</sup>) microtubules, 3 independent experiments. Asterisks indicate Mann-Whitney  $U$  test significance values.  $***P < 10^{-4}$ . **(D)** Time series showing the breaking of a microtubule (green) upon application of fluid flow. Large beads nonspecifically adhering to the surface (arrowhead) were used as fixed obstacles to enhance microtubule bending upon flow thus resulting in microtubule rupture at the site of maximal bending. Scale bar: 10  $\mu$ m. **(E)** Time taken for microtubules to break after application of flow. The shortest experimental application of flow was 9.55 s and all microtubules not broken at 9.55 s are displayed as dots.  $N = 46$  (Ac<sup>1</sup>) and 42 (Ac<sup>97</sup>) microtubules, 2 independent experiments. The frequency of breakage is 28% for Ac<sup>1</sup> microtubules and 2% for Ac<sup>97</sup> microtubules. A Mann-Whitney  $U$  test was conducted on the entire data set and asterisks indicate significance values.  $**P < 0.005$ . **(F)** Model for regulation of microtubules mechanics by TAT1-mediated acetylation. We propose a two-step adaptive model for the mechanical stabilization of microtubules where bending results in sidewall breathing and lets TAT1 enter the lumen. Subsequent acetylation locally modifies the mechanical properties of the microtubule to protect it against flexural breakage.